How to cite: *Angew. Chem. Int. Ed.* **2021**, *60*, 8896–8904
International Edition: doi.org/10.1002/anie.202016592
German Edition: doi.org/10.1002/ange.202016592

VIP **Porous Materials** **Very Important Paper**

Chiral Self-sorting of Giant Cubic [8+12] Salicylimine Cage Compounds

*Philippe Wagner, Frank Rominger, Wen-Shan Zhang, Jürgen H. Gross, Sven M. Elbert, Rasmus R. Schröder, and Michael Mastalerz**

Abstract: *Chiral self-sorting is intricately connected to the complicated chiral processes observed in nature and no artificial systems of comparably complexity have been generated by chemists. However, only a few examples of purely organic molecules have been reported so far, where the self-sorting process could be controlled. Herein, we describe the chiral self-sorting of large cubic [8+12] salicylimine cage compounds based on a chiral TBTQ precursor. Out of 23 possible cage isomers only the enantiopure and a meso cage were observed to be formed, which have been unambiguously characterized by single crystal X-ray diffraction. Furthermore, by careful choice of solvent the formation of meso cage could be controlled. With internal diameters of $d_{in} = 3.3–3.5$ nm these cages are among the largest organic cage compounds characterized and show very high specific surface areas up to approx. 1500 $m^2 g^{-1}$ after desolvation.*

Introduction

Chiral self-sorting refers to the high-fidelity recognition of self from non-self within racemic mixtures of enantiomers. If one enantiomer shows higher affinity for the opposite enantiomer than for the same enantiomer, the process is called chiral social self-sorting (self-discrimination); if it shows higher affinity for the same enantiomer, it is called chiral narcissistic self-sorting (or self-recognition).[1] Chiral self-sorting has been recognized to be relevant to important biological processes such as amyloidogenesis (toxic misfolding of proteins).[1a,2] Even the compartmentalization of different functional architectures in a cell, which is essential for life, can be viewed as a very complex example of (chiral) self-sorting.[3] Furthermore, chiral self-sorting, especially in combination with autocatalysis, may have played a crucial role in the origin of biological homochirality.[1a,4]

Artificial systems have not nearly reached the degree of complexity present in nature. Nevertheless, some fascinating systems which display chiral self-sorting with high selectivity have been realized.[1a] The majority of the systems reported in literature are based on noncovalent interactions such as electrostatic interactions,[5] π stacking,[6] hydrogen bonding[7] and coordination bonds.[8] In the context of dynamic covalent chemistry (DCC),[9] zirconocene coupling,[10] alkyne metathesis,[11] disulfide bond formation,[12] imine condensation[13] and boronic ester formation[14] have been used to study chiral self-sorting. More fascinating, a few examples of more complex systems have been reported where DCC in combination with noncovalent interactions have been investigated for self-sorting. For instance, based on a combination of π stacking and disulfide bond formation the chiral self-sorting of twisted perylene stereodimers occurred.[15] The same combination of π stacking and disulfide formation was exploited to synthesize a *meso* figure-of-eight knot in 90% yield from racemic precursors.[16] Another example is relying on hydrogen bonding together with imine condensation for the self-sorting to hybrid peptide capsules.[17]

In recent years, a large number of different organic cages varying in size and geometries based on imine and boronic ester condensation were realized by using relative simple precursors.[18] The intrinsic reversibility of the bond formation allows to study the thermodynamics of cage synthesis and gives an opportunity to gain fundamental insight into self-sorting processes.[8,13,14,19,20] Despite the increasing number of studied self-sorting processes during cage formation and the fundamental knowledge gained by it, the number of examples where complexity is increased simply by chiral self-sorting DCC cages is relatively scarce.[13,14] The largest imine cage compounds formed by chiral self-sorting to date are [4+6] cages.[13g] These are based on the condensation of six chiral 1,2-diphenylethylene diamines and four truxene trialdehydes. Since the truxene is prochiral, an astonishing (narcissistic) self-sorting process has been observed, where only two enantiomeric cages out of 123 possible structures are formed. It is worth mentioning that Warmuth and co-workers reported on early attempts to study the chiral self-sorting of larger [8+12] cubic cages, but unfortunately at that time were unsuccessful.[21] To the best of our knowledge, for none of the larger systems any control of self-sorting process, for example,

[*] M. Sc. P. Wagner, Dr. F. Rominger, Dr. J. H. Gross, Dr. S. M. Elbert, Prof. Dr. M. Mastalerz
Organisch-Chemisches Institut
Ruprecht-Karls-Universität Heidelberg
Im Neuenheimer Feld 270, 69120 Heidelberg (Germany)
E-mail: michael.mastalerz@oci.uni-heidelberg.de
Dr. W.-S. Zhang, Prof. Dr. R. R. Schröder
Centre for Advanced Materials
Ruprecht-Karls-Universität Heidelberg
Im Neuenheimer Feld 225, 69120 Heidelberg (Germany)
Supporting information and the ORCID identification number(s) for the author(s) of this article can be found under: https://doi.org/10.1002/anie.202016592.

switching between narcissistic or social, has been achieved. In this respect, our previous contribution of chiral self-sorting of [2+3] cages is still the largest and most complex system studied to date.[13i]

Here we report on the chiral self-sorting of giant cubic [8+12] salicylimine cages, based on the condensation of eight chiral C_3-symmetric TBTQ-tris(salicylaldehydes) with 12 *p*-phenylenediamines; the largest number of components used so far, especially in respect to control social or narcissistic events.

Results and Discussion

For the synthesis of the cubic cages, first chiral TBTQ-based salicylaldehydes **2** were synthesized by Duff-formylation[22] of the C_3-symmetric triols **1** (Scheme 1).[23] Whereas racemic TBTQ (±)-**1** gave the corresponding tris(salicylaldehyde) (±)-**2** in 51 % yield; the yield was a bit lower for the conversion of enantiopure C_3-symmetric (−)-(*P*)-**1** and (+)-(*M*)-**1** giving (−)-(*P*)-**2** and (+)-(*M*)-**2** in 41 % and 40 %, respectively.

Before studying the self-sorting during cage formation by using racemic salicylaldehyde (±)-**2** and 1,4-phenylenediamine **3**, we investigated the stoichiometric reaction between enantiopure salicylaldehyde (+)-(*M*)-**2** and amine **3** in different deuterated solvents using 12 mol % TFA as a catalyst (Scheme 2).

In all solvents (dichloromethane-D_2, $CDCl_3$, tetrachloroethane-D_2, THF-D_8, 1,4-dioxane-D_8, [D_6]DMSO), the desired [8+12] cage compound (*M*)-**4** was identified as main product by ^{1}H NMR and MALDI-TOF mass spectrometry (calcd for $C_{352}H_{337}N_{24}O_{24}$ $[M+H]^+$: 5286.60, found: 5287.04) (Figure 1). In CD_2Cl_2, the reaction occurred most cleanly and only signals of the desired cage compound and no side products were visible in the ^{1}H NMR spectrum (Figure 2). A ^{1}H DOSY NMR spectrum of the cage compound (*M*)-**4** in dichloromethane-D_2 showed only one trace of signals with a diffusion coefficient of $D = 3.40 \times 10^{-10}$ m^2 s^{-1} corresponding to a solvodynamic radius of 1.55 nm, which is in good agreement with the inner diameter of 3.3–3.5 nm of the [12+8] cage compound found by single crystal X-ray diffraction (vide infra).

Running the cage formation reaction at room temperature revealed significant differences in the reaction rate depending on the solvent used: in CD_2Cl_2 after 18 h almost full conversion to the cage compound was observed whilst in

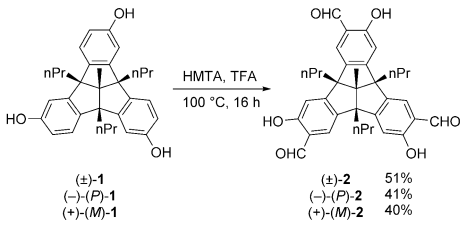

Scheme 1. Synthesis of the racemic and enantiopure C_3-symmetric TBTQ-tris(salicylaldehydes) (±)-**2**, (−)-(*P*)-**2** and (+)-(*M*)-**2** by Duff-formylation of the corresponding TBTQ-tris(phenols).

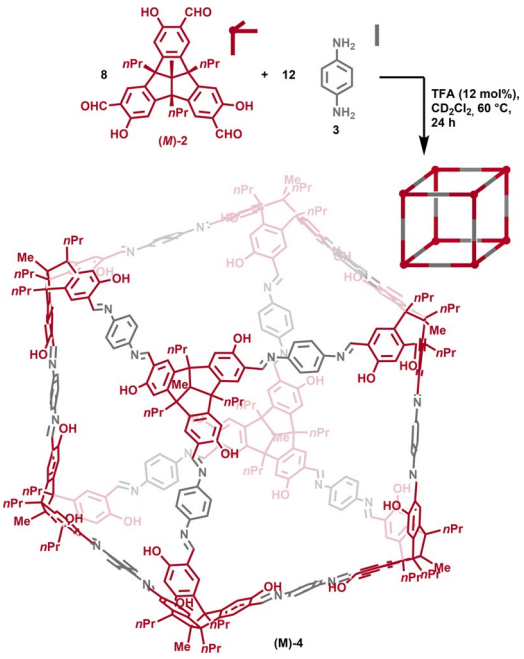

Scheme 2. Condensation of the enantiopure tris(salicylaldehyde) (*M*)-**2** with *p*-phenylenediamine **3** leading to the chiral cubic [8+12] imine cage compound (*M*)-**4**. The cage compound is also represented schematically as cube with the chiral TBTQ-units in red and the linear *p*-phenylenediimine linkers at the edges in grey.

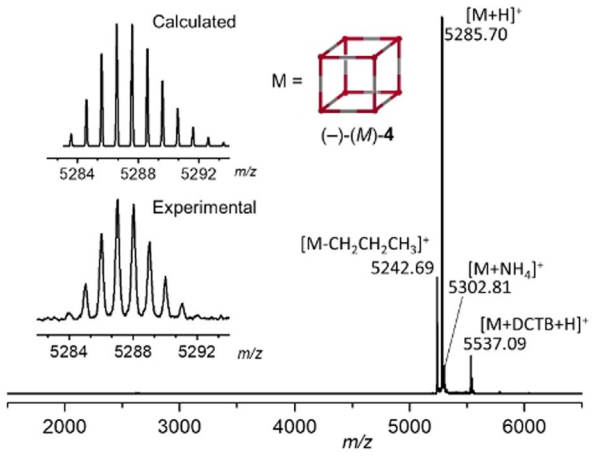

Figure 1. MALDI-TOF mass spectrum (matrix: DCTB; overview: linear mode, isotopic pattern: reflector mode) of the [8+12] cage (*M*)-**4** from CD_2Cl_2).

$CDCl_3$ only cage intermediates were visible after the same time and only after heating the reaction to 50 °C the reaction was complete (see Figure S25 in the Supporting Information). Based on these observations, dichloromethane was used for the synthesis of the enantiopure cage compounds (*P*)-**4** and (*M*)-**4** on larger scales, which could be isolated in 94 % and 98 % yield, respectively. It is worth mentioning that the synthesis of pure samples of (*P*)-**4** and (*M*)-**4** was difficult, since attempts to purify the crude reaction product by precipitation with methanol, acetonitrile or *n*-pentane inevitably resulted in a precipitate that was nearly insoluble in all solvents. However, by carefully controlling the stoichiometry,

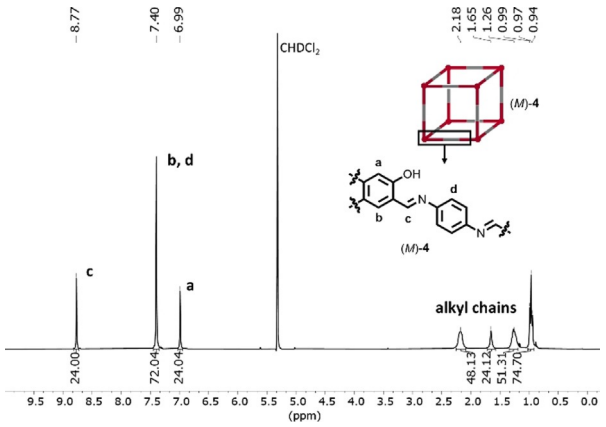

Figure 2. ^{1}H NMR spectrum (300 MHz) of (*M*)-**4** in CD_2Cl_2, no signal is visible for the OH protons because of the presence of TFA.

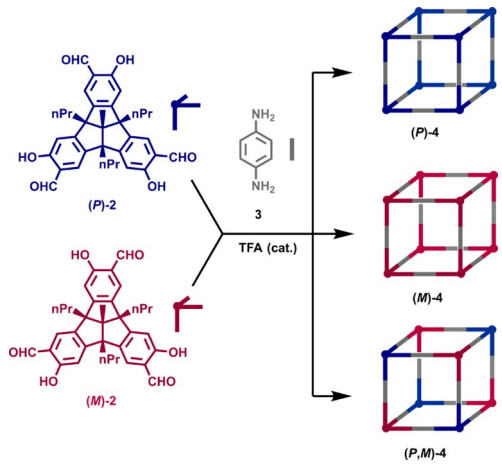

Scheme 3. Condensation of the tris(salicylaldehyde) **2** with *p*-phenylenediamine **3** leading to the cubic [8+12] imine cage compounds (*P*)-**4**, (*M*)-**4** and (*P,M*)-**4**. The cage compounds are represented schematically as cubes with the TBTQ-units at their vertices in blue for the (*P*)-enantiomer, in red for the (*M*)-enantiomer and the linear *p*-phenylenediimine linkers at the edges in grey.

pure samples of the [8+12] cage compounds (*P*)-**4** and (*M*)-**4** were obtained by neutralizing the catalytic amount of TFA used in the reaction with solid $NaHCO_3$ and removing the solvent under reduced pressure.

The enantiopure cage compounds (+)-(*P*)-**4** and (−)-(*M*)-**4** possess very large molar optical rotations of $[\Phi] \geq \pm 13\,000 \times 10°\ cm^2\,mol^{-1}$.[24] Circular dichroism (CD) spectra of (+)-(*P*)-**4** and (−)-(*M*)-**4** are mirror-imaged and also show very large molar extinctions of $\Delta\varepsilon \geq \pm 800\ M^{-1}\,cm^{-1}$, however, since the UV/Vis absorption is also quite large, more modest values for the dissymmetry factor are obtained ($g_{abs} = 0.005$) (Figure 3).[13e,25] To our knowledge only two cages with a stronger Cotton effect have been reported in literature: a face-rotating polyhedron by the group of Cao ($\Delta\varepsilon = \pm 1395$)[13e] and a cubic cage by Warmuth and co-workers ($\Delta\varepsilon = \pm 7277$).[21] The nearly 10-fold higher value of the latter in comparison to our system is interesting, because the described cages have comparable dimensions and a very similar chromophore.

To study the chiral self-sorting (see Scheme 3), the condensation reaction of racemic salicylaldehyde (±)-**2** and diamine **3** was carried out in different solvents and after workup the reaction mixture was investigated by ^{1}H NMR spectroscopy in $CDCl_3$ (see Figure S26 in the Supporting Information). Again, in DCM the reaction is the cleanest, showing two relatively sharp imine derived signals at $\delta = 8.71$ and 8.68 ppm and a few minor peaks in this region, which are caused by oligomeric intermediates (see ^{1}H DOSY NMR in Figure S27 and mass spectrum in Figure S28 in the Supporting Information). By comparing the chemical shifts with those of the isolated, pure cage (*M*)-**4**, the imine derived signal at 8.71 ppm was clearly assigned to a racemic mixture of the enantiopure cages (*P*)-**4** and (*M*)-**4** and the signal at 8.68 ppm tentatively to the *meso* cage (*P,M*)-**4** (Figure 4). These results indicate, that in DCM social self-sorting leading to the *meso* cage compound (*P,M*)-**4** is slightly favoured over narcissistic self-sorting ((*P*/*M*)-**4**:(*P,M*)-**4** = 45:55). In other solvents investigated ($CDCl_3$, THF, 1,4-dioxane, [D_6]DMSO), broad

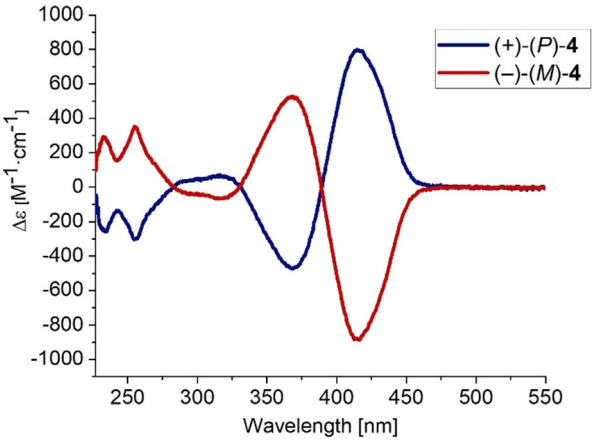

Figure 3. CD spectra of the [8+12] cage compounds (+)-(*P*)-**4** and (−)-(*M*)-**4** in CH_2Cl_2 at 20 °C ($c = 1.74 \times 10^{-6}$ M for (+)-(*P*)-**4** and 1.93×10^{-6} M for (−)-(*M*)-**4**).

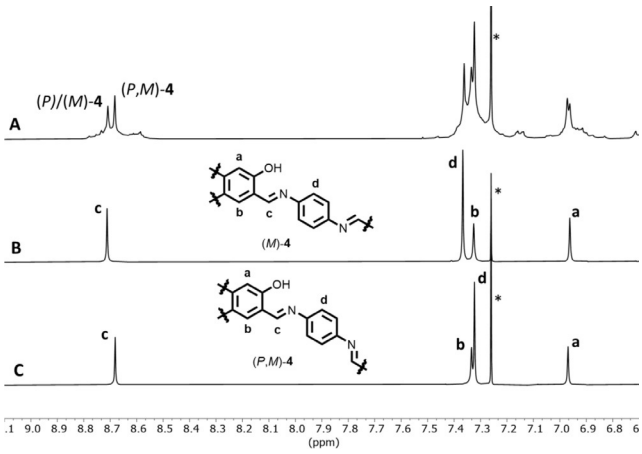

Figure 4. Comparison of ^{1}H NMR spectra ($CDCl_3$, A: 400 MHz, B, C: 600 MHz) of: A) of the reaction of a mixture of (±)-**2**, p-phenylenediamine **3** (1.5 equiv) and TFA (12 mol%) heated at 60 °C for 24 h in dichloromethane, B) isolated enantiopure cage compound (*M*)-**4**, C) isolated *meso* cage compound (*P,M*)-**4**; * $CHCl_3$.

signals indicative of undefined oligomers were detected alongside with the characteristic cage signals, making a quantitative evaluation of the results impossible (see Figure S26). The reversibility of the cage formation by heating a 1:1 mixture of (*P*)-**4** and (*M*)-**4** in CD_2Cl_2 was investigated. In the presence of TFA and water no formation of the (*P*,*M*)-**4** cage was found. Only after adding a small amount of *p*-phenylenediamine a reaction occurred and characteristic signals of the *meso* cage (*P*,*M*)-**4** could be detected.

According to Burnside's lemma,[26] 23 cage isomers (including enantiomers) are possible (see Chapter 16 in the Supporting Information). By semi-empirical calculations (PM6) the enthalpies of formation (ΔH_R) of all possible isomers were calculated (Figure 5, see also Table S4 and Figure S79 in the Supporting Information), identifying the ones with the highest symmetry numbers as enthalpically

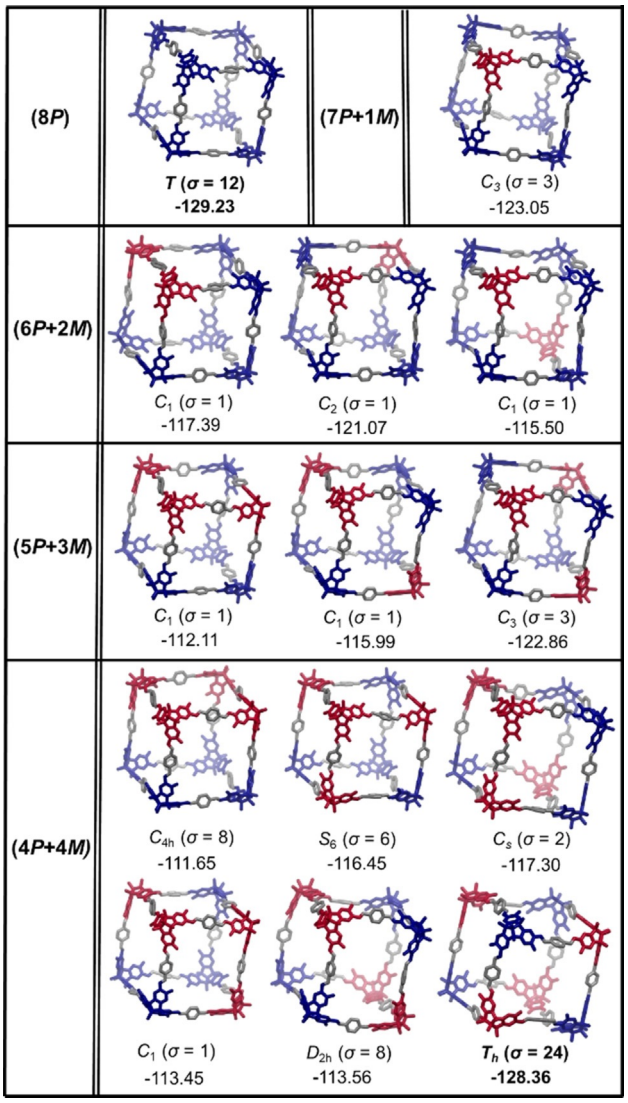

Figure 5. PM6 optimized models of the possible cage isomers (enantiomers not included), their point group symmetry, symmetry number σ and enthalpies of formation (ΔH_R) [kJ mol^{-1}]. In bold the numbers for the experimentally observed cages are highlighted. Propyl were reduced to methyl chains; blue: (*P*)-enantiomer, red: (*M*)-enantiomer, grey: *p*-phenylenediimine linkers.

favoured.[27] These are exactly the two cages, which are formed in the reaction as major compounds, namely the enantiopure (*P*)-**4** (*T* symmetry, $\sigma = 12$, $\Delta H_R = -129.23$ kJ mol^{-1}) and the *meso*-cage (*P*,*M*)-**4** (T_h, $\sigma = 24$; $\Delta H_R = -128.36$ kJ mol^{-1}). According to the difference of $|\Delta\Delta H_R| = 0.87$ kJ mol^{-1} a distribution between these three cages is assumed to be 58:42[28] if entropic factors are neglected, which is close to the observed distribution of 45:55. For certain, entropy plays a role as well as solvation effects, but these are difficult to accurately quantify or calculate.[29] However, the experimental data suggests a strong correlation between the symmetry of the cage compounds and their observed ratios, which cannot solely be explained by enthalpic factors. According to information theory, a loss of information leads to an increase in entropy and according to this theory, the maximum of entropy of any system corresponds to the highest symmetry (and lowest amount of information).[30] This is in accordance with the observation made for the self-sorting of other cages or (macrocycles) applying DCC.[11,31] Thus it is assumed, that the two major formed cage products are not only enthalpically but also entropically favoured products.

In THF at room temperature, the formation of a small amount of yellow precipitate was observed, which was unambiguously identified as the *meso* [8+12] cage compound (*P*,*M*)-**4**. This suggested, that the lower solubility of the *meso* cage can be used to drive the equilibrium towards social self-sorting and to isolate the pure cage compound (*P*,*M*)-**4**; a strategy that has already previously been employed by our group.[13i,19c] After optimization of the reaction conditions of salicylaldehyde (±)-**2** and phenylenediamine **3** (12 mol% TFA, dry THF, 10 days), *meso*-cage (*P*,*M*)-**4** was isolated by filtration and washing with *n*-pentane in 83% yield. The precipitate obtained by this route was completely soluble in chloroform, indicating the absence of any insoluble imine polymers as side-products (see Figure S87 in the Supporting Information).

Slow evaporation of $CDCl_3$ from an NMR sample containing the [8+12] cage compounds (*P*,*M*)-**4** and (*P*/*M*)-**4** resulted in cubic crystals which were identified as the *meso* [8+12] cage compound (*P*,*M*)-**4** by single crystal X-ray diffraction analysis (Figure 6). The crystals contain large amounts of disordered solvate molecules (approx. 76% of the unit cell volume), for which the electron density was removed by using the SQUEEZE function of PLATON.[32] The refinement was carried out using geometric local symmetry restraints and the phenyl rings have been treated as rigid hexagons. Additionally, rigid bond restraints were applied to control atomic displacement parameters. (*P*,*M*)-**4** crystallizes in the cubic space group $Ia\bar{3}$ with eight molecules of (*P*,*M*)-**4** per unit cell. The molecule itself shows $\bar{3}$-symmetry. The cavity of (*P*,*M*)-**4** has an inner diameter of 3.3 nm (measured between the apical carbon atoms of two opposite TBTQ-units) and thus the cube has a void volume of about 6.9 nm^3. With these cage dimensions, (*P*,*M*)-**4** is one of the largest purely organic cages reported that has been characterized by X-ray diffraction; similar in size to the boronic ester cage of our group ($d_{in} = 3.1$ nm),[33] but smaller than the recently published resorcinarene based cages from the Yuan group

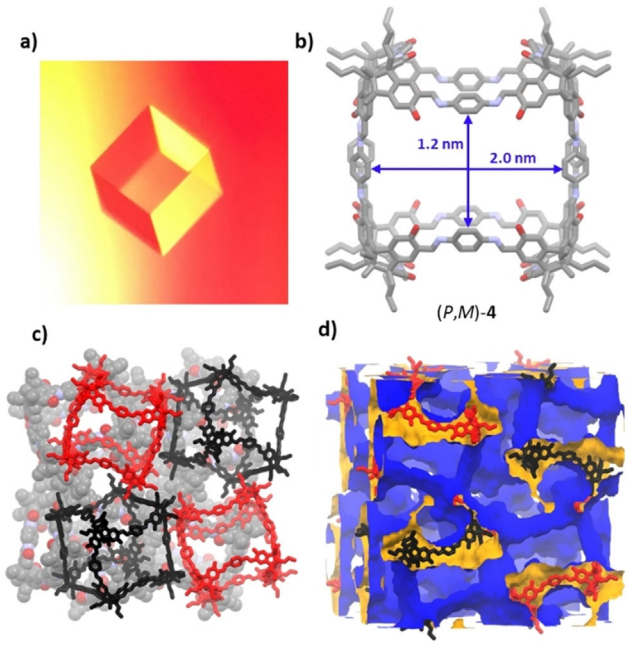

Figure 6. a) light microscope image (×40) of a cubic crystal of (*P*,*M*)-**4**; b) X-ray single crystal structure of an independent molecule of (*P*,*M*)-**4** and cage window size, hydrogen atoms were omitted for clarity; grey: carbon, red: oxygen, violet: nitrogen; c) packing in the solid state, cage molecules were colored in red and black for clarity; d) voids in the crystal (contact surface) shown in blue and orange, cage molecules alternating in red and black (created with Mercury 4.3.1, 2020, probe radius: 1.82 Å, grid spacing 0.7 Å).[43]

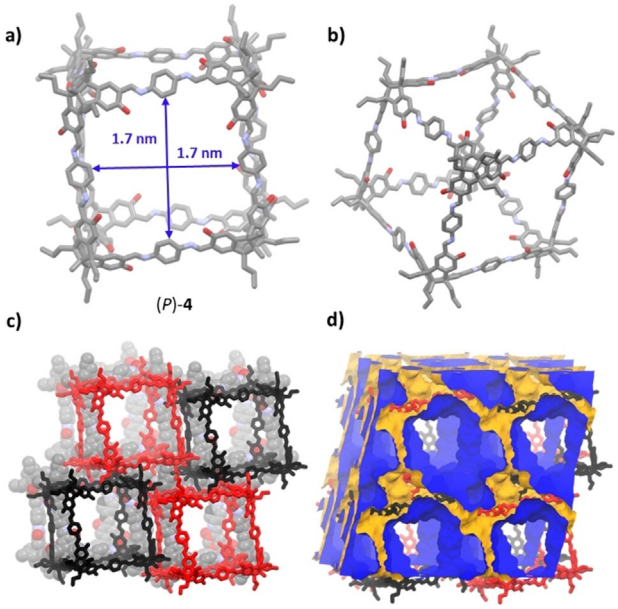

Figure 7. a) X-ray single crystal structure of an independent molecule of (*P*)-**4** and cage window size, hydrogen atoms were omitted for clarity; grey: carbon, red: oxygen, violet: nitrogen; b) (*P*)-**4** highlighting the symmetry of the molecule; c) packing in the solid state, cage molecules were colored in red and black for clarity; d) voids in the crystal (contact surface) shown in blue and orange, cage molecules alternating in red and black (created with Mercury 4.3.1, 2020, probe radius: 1.82 Å, grid spacing 0.7 Å).[43]

($d_{in} = 3.9$ nm)[34] and the giant porphyrinic cages from Kimoon Kim and co-workers ($d_{in} = 4.3$ nm).[35] The rectangular cage window is exceptionally large with a size of approx. 2.0 × 1.2 nm (measured between opposite aryl rings) and a diameter of 2.3 nm (Figure 6b) and only the giant porphyrinic cages from Kimoon Kim and co-workers have slightly larger cage windows of approximately 1.8 × 1.5 nm.[35] The molecules pack through weak van der Waals interactions between the edges of adjacent cage molecules involving the propyl-chains and apical methyl-groups of the TBTQ-units of one cage and the aryl rings and phenolic OH groups of the other cage (Figure 6c). Crystals of the *meso* cage compound (*P*,*M*)-**4** grown from dichloromethane were isomorphic to those grown from $CDCl_3$ with the exception that the cell parameters are slightly different (for details, see Supporting Information).

Suitable single-crystals of the enantiopure [8+12] cage compound (*P*)-**4** for X-ray diffraction were grown by slow evaporation of a concentrated solution of (*P*)-**4** in CD_2Cl_2 at room temperature (Figure 7). Again, the crystals contain large amounts of disordered solvent molecules (approx. 69 % of the unit cell volume), for which the electron density was removed by using the SQUEEZE function of PLATON.[32] The compound crystallizes in the triclinic space group *P*1 with one cage molecule per unit cell. The inner diameter of (*P*)-**4** is similar to the one of *meso* cage (*P*,*M*)-**4** with a value between 3.3–3.5 nm ($V_{in} \approx 6.9$ nm^3) and the cage window is rhombic with a size of 1.7 nm^2 (measured between opposite aryl rings) (Figure 7a). This makes (*P*)-**4** the largest chiral purely organic cage reported that has been characterized by X-ray diffraction, considerably larger than a chiral imine cage from the group of Cooper ($V_{in} \approx 1.5$ nm^3).[29b] The antiperiplanar arrangement of the imine substituents of the *p*-phenylenediimine units in (*P*)-**4** results in a three-dimensional structure with the shape of a rhombohedron with an angle of $\theta \approx 100$–110°. The packing motif of the enantiopure cage compound (*P*)-**4** is considerably more complex than for the *meso* cage (*P*,*M*)-**4** and consist of various van der Waals interactions between adjacent cage molecules. Most importantly, in comparison to the *meso* cage (*P*,*M*)-**4**, the cage molecules are not twisted at an angle against each other and pack much more densely (Figure 7c). Due to the denser packing no extrinsic pores are formed between adjacent cage molecules (Figure 7d).

While it has been previously shown that chirality can have a large influence on the porosity of organic cage compounds,[13i,36] this is the first time, that the crystal structure of an enantiopure cage and also of the corresponding achiral *meso* cage have been solved by single crystal X-ray diffraction and a direct comparison of their packing motifs has been possible. However, these cages are not only chiral and achiral congeners but also among the largest ones reported by single-crystal X-ray diffraction. Cages of this size, especially if they possess large cage windows, like the recently published porphyrinic cages of Kimoon Kim,[35] have been reported to loose crystallinity and porosity upon desolvation.[29b,31,35,37] Therefore, we were curious if these materials can be activated for gas sorption. Analysing the crystal structures with CrystalExplorer (isovalue: 0.0003 au)[38] revealed exceptionally high virtual porosities of 4726 m^2 g^{-1} for (*P*,*M*)-**4** (Fig-

ure 6d) and 3830 $m^2 g^{-1}$ for (*P*)-**4** (Figure 7d). To investigate the gas sorption properties, the [8+12] cage compounds (*P,M*)-**4**, (*P*)-**4** and (*M*)-**4** were thermally activated at 100 °C under vacuum. For *meso* cage (*P,M*)-**4**, in addition to the precipitate formed during the reaction ((*P,M*)-**4**_1), a sample ((*P,M*)-**4**_2) of crystalline material was prepared by slow evaporation of solvent of a saturated solution of (*P,M*)-**4** in $CHCl_3$. Here, the crystalline sample was activated by solvent exchange with *n*-pentane (3 × 48 h) and evacuating at room temperature to prevent thermal stress.[39]

TGA measurements confirmed the loss of solvent molecules and showed stabilities up to 400 °C. PXRD measurements indicated that (*P,M*)-**4**_2 possesses the highest degree of crystallinity of all four samples (see Supporting Information), which was confirmed by scanning electron microscopy (SEM), showing that (*P,M*)-**4**_1, (*P*)-**4** and (*M*)-**4** are composed of amorphous and crystalline particles, whereas (*P,M*)-**4**_2 contains a high proportion of crystalline material (Figure 8). By nitrogen sorption at 77 K all samples showed type-I isotherms with specific surface areas (Brunauer-Emmett-Teller model) of $SA_{BET} = 1134\ m^2 g^{-1}$ for (*P,M*)-**4**_1 and $SA_{BET} = 1487\ m^2 g^{-1}$ for (*P,M*)-**4**_2, demonstrating that morphology and crystallinity plays an important role. The more crystalline sample being more porous. As expected, the two enantiomeric cages (*P*)-**4** ($SA_{BET} = 1212\ m^2 g^{-1}$) and (*M*)-**4** ($SA_{BET} = 1126\ m^2 g^{-1}$) show almost identical gas sorption behaviour (Figure 8). QSDFT calculations (N_2 at 77 K on carbon, cylindrical/spherical pores, QSDFT absorption branch, fitting errors: 1.2–1.6 %) gave pore diameters of the four samples between 1.6–1.7 nm, which are related to the window sizes of the cages. The adsorption of other gases (CH_4 and CO_2) was also investigated (for details, see Table 1 and Supporting Information) and gas uptakes (in wt.-%), Henry (S_H) as well as IAST selectivities were calculated. (*P*)-**4**, (*M*)-**4** and the less crystalline (*P,M*)-**4**_1, which have comparable N_2-isotherms and SA_{BET}'s, also show comparable Henry and IAST selectivities. For instance, S_H (CO_2/CH_4) is between 7.1 and 7.6 and S_H (CO_2/N_2) is between 24.7 and 28.0. The IAST selectivities for CO_2/CH_4 (50:50) and CO_2/N_2 (20:80) at 273 K are in a comparable range and show no strong pressure

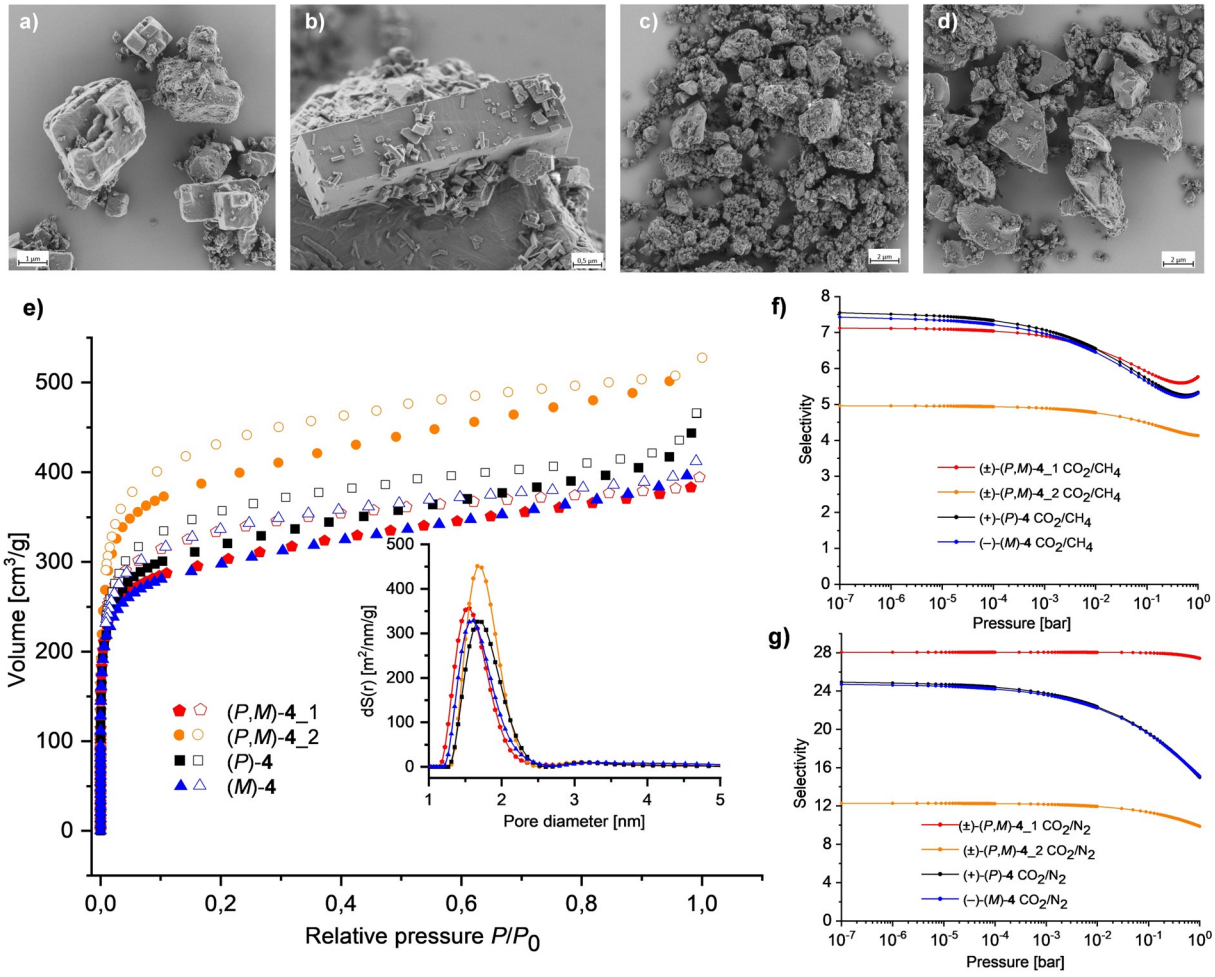

Figure 8. SEM images of a) (*P,M*)-**4**_1 (precipitate formed during the reaction), b) (*P,M*)-**4**_2 (crystals grown from $CHCl_3$), c) (*P*)-**4**, d) (*M*)-**4**; e) Nitrogen isotherms at 77 K and QS-DFT pore size distribution plots (N_2 at 77 K on carbon, cylindrical/spherical pores, QSDFT absorption branch) of the [8+12] cage compounds, red pentagons: (*P,M*)-**4**_1, orange circles: (*P,M*)-**4**_2, black squares: (*P*)-**4**, blue triangles: (*M*)-**4**; f) IAST selectivity curves of the [8+12] cage compounds for CO_2/CH_4 (50:50) at 273 K and g) for CO_2/N_2 (20:80) at 273 K (red curve: (*P,M*)-**4**_1, orange curve: (*P,M*)-**4**_2, black curve: (*P*)-**4**, blue curve: (*M*)-**4**); the selectivity at 1×10^{-7} bar corresponds to the Henry selectivity.

Table 1: Summary of crystal structure derived properties and experimental gas sorption properties (BET derived surface areas, selectivities, gas uptakes and heats of adsorption) of the [8+12] cage compounds (*P,M*)-**4_1** (precipitate formed during the reaction), (*P,M*)-**4_2** (crystals grown from $CHCl_3$), (*P*)-**4** and (*M*)-**4**.

Cage	Inner diameter [nm][a]	Cage window size [nm][b]	Virtual porosity [$m^2 g^{-1}$][c]	SA_{BET} [$m^2 g^{-1}$][d]	Henry selectivity (CO_2/CH_4)[e]	Henry selectivity (CO_2/N_2)[f]	Uptake in wt.-% at 1.0 bar		Q_{st} (CO_2) [kJ mol^{-1}][g]	Q_{st} (CH_4) [kJ mol^{-1}][g]
							CO_2 (273 K)	CH_4 (273 K)		
(*P,M*)-**4**_1	3.3	2.0×1.2	4726	1134	7.1	28.0	12.41	1.36	29.3	25.9
(*P,M*)-**4**_2				1487	5.0	12.3	14.61	1.70	25.4	–[h]
(*P*)-**4**	3.3–3.5	1.7×1.7	3830	1212	7.6	24.9	12.01	1.30	24.2	17.8
(*M*)-**4**				1126	7.4	24.7	12.50	1.41	25.0	14.0

[a] Measured between the apical carbon atoms of two opposite TBTQ-units; [b] measured between opposite aryl rings; [c] calculated with CrystalExplorer, isovalue: 0.0003 au, very low resolution; [d] BET derived surface areas for N_2 at 77 K; [e] calculated for a hypothetical 50:50 mixture of CO_2:CH_4; [f] calculated for a hypothetical 20:80 mixture of CO_2:N_2; [g] zero coverage heat of adsorption; [h] the isotherm could not be adequately fitted.

dependency. This, together with the moderate heats of adsorption (Q_{st} = 24.2–29.3 kJ mol^{-1} for CO_2 and 14.0–25.9 kJ mol^{-1} for CH_4), indicates that the cages have no adsorption sites that strongly bind CO_2 or CH_4.

It is more interesting to compare (*P,M*)-**4**_1and (*P,M*)-**4**_2. The latter is more crystalline and has a higher specific surface area, but is less selective (S_H (CO_2/CH_4) = 5.0 vs. 7.1 and S_H (CO_2/N_2) = 12.3 vs. 28.0) once more emphasizing that a higher ordered crystalline material is not necessarily better than an amorphous one in terms of materials properties.[36a,40]

Conclusion

To summarize, we have investigated the chiral self-sorting of large cubic [8+12] salicylimine cage compounds formed by condensation of eight chiral C_3-symmetric TBTQ-tris(salicylaldehydes) with 12 *p*-phenylenediamine, the largest number of components used so far in a chiral self-sorting system. Out of 23 possible cage isomers only the three isomers (*P*)-**4**, (*M*)-**4** and (*P,M*)-**4** were found to be formed ((*P/M*)-**4**:(*P,M*)-**4** = 45:55). This high selectivity of the chiral self-sorting can be explained by a combination of enthalpic and entropic factors, which both favour the cage compounds with the highest degree of symmetry. Despite the small differences in energy between the favoured cages and the unprecedented complexity of the system, we were able to control the self-sorting process and isolate the *meso* cage (*P,M*)-**4** in 83% yield by taking advantage of its lower solubility. To the best of our knowledge, this control between narcissistic and social self-sorting is unprecedented for cages of this size and has been described prior only for smaller [2+3] imine cages.[13i] The *meso* cage as well as the enantiopure cage were characterized by X-ray diffraction and are among the largest organic cages characterized by this method and the largest chiral ones. Gas sorption measurements revealed high specific surface areas of up to SA_{BET} = 1487 $m^2 g^{-1}$ (N_2, 77 K), a value that has been rarely exceeded by other cages reported so far.[33,34,41] Interestingly, the most crystalline sample displayed the highest specific surface area but the lowest selectivities, emphasizing that crystallinity and high degree of order does not necessarily lead to superior gas sorption properties.[41a,42]

Acknowledgements

We thank the European Research Council ERC in the frame of the consolidators grant CaTs n DOCs (grant no. 725765) and acknowledge support by the state of Baden Württemberg through bwHPC and the German Research Foundation (DFG) through grant no INST 40/575 1 FUGG (JUSTUS 2 cluster). Open access funding enabled and organized by Projekt DEAL.

Conflict of interest

The authors declare no conflict of interest.

Keywords: cage compounds · chiral · imine · self-sorting · tribenzotriquinacene

[1] a) H. Jędrzejewska, A. Szumna, *Chem. Rev.* **2017**, *117*, 4863–4899; b) C. Li, Y. Zuo, Y.-Q. Zhao, S. Zhang, *Chem. Lett.* **2020**, *49*, 1356–1366.

[2] a) W. P. Esler, E. R. Stimson, J. B. Fishman, J. R. Ghilardi, H. V. Vinters, P. W. Mantyh, J. E. Maggio, *Biopolymers* **1999**, *49*, 505–514; b) T. Koga, M. Matsuoka, N. Higashi, *J. Am. Chem. Soc.* **2005**, *127*, 17596–17597; c) V. Torbeev, M. Grogg, J. Ruiz, R. Boehringer, A. Schirer, P. Hellwig, G. Jeschke, D. Hilvert, *J. Pept. Sci.* **2016**, *22*, 290–304.

[3] M. M. Safont-Sempere, G. Fernández, F. Würthner, *Chem. Rev.* **2011**, *111*, 5784–5814.

[4] a) S. Jaakkola, V. Sharma, A. Annila, *Curr. Chem. Biol.* **2008**, *2*, 153–158; b) I. Rubinstein, R. Eliash, G. Bolbach, I. Weissbuch, M. Lahav, *Angew. Chem. Int. Ed.* **2007**, *46*, 3710–3713; *Angew. Chem.* **2007**, *119*, 3784–3787; c) A. Saghatelian, Y. Yokobayashi, K. Soltani, M. R. Ghadiri, *Nature* **2001**, *409*, 797–801.

[5] a) A. M. Costero, M. Colera, P. Gaviña, S. Gil, L. E. Ochando, *New J. Chem.* **2006**, *30*, 1263–1266; b) M. Wierzbicki, A. Szumna, *Chem. Commun.* **2013**, *49*, 3860–3862.

[6] a) N.-T. Lin, A. Vargas Jentzsch, L. Guénée, J.-M. Neudörfl, S. Aziz, A. Berkessel, E. Orentas, N. Sakai, S. Matile, *Chem. Sci.* **2012**, *3*, 1121–1127; b) M. M. Safont-Sempere, P. Osswald, M. Stolte, M. Grüne, M. Renz, M. Kaupp, K. Radacki, H. Braunschweig, F. Würthner, *J. Am. Chem. Soc.* **2011**, *133*, 9580–9591; c) N. Saito, R. Terakawa, M. Yamaguchi, *Chem. Eur. J.* **2014**, *20*, 5601–5607.

[7] a) M. Suárez, N. Branda, J.-M. Lehn, A. Decian, J. Fischer, *Helv. Chim. Acta* **1998**, *81*, 1–13; b) L. J. Prins, J. Huskens, F. de Jong,

P. Timmerman, D. N. Reinhoudt, *Nature* **1999**, *398*, 498 – 502; c) W. Makiguchi, J. Tanabe, H. Yamada, H. Iida, D. Taura, N. Ousaka, E. Yashima, *Nat. Commun.* **2015**, *6*, 7236; d) E. Huerta, S. A. Serapian, E. Santos, E. Cequier, C. Bo, J. de Mendoza, *Chem. Eur. J.* **2016**, *22*, 13496 – 13505; e) M. Alajarin, R.-A. Orenes, J. W. Steed, A. Pastor, *Chem. Commun.* **2010**, *46*, 1394 – 1403; f) K. Aratsu, R. Takeya, B. R. Pauw, M. J. Hollamby, Y. Kitamoto, N. Shimizu, H. Takagi, R. Haruki, S.-i. Adachi, S. Yagai, *Nat. Commun.* **2020**, *11*, 1623.

[8] a) T. Tateishi, T. Kojima, S. Hiraoka, *Commun. Chem.* **2018**, *1*, 20; b) T. Kamada, N. Aratani, T. Ikeda, N. Shibata, Y. Higuchi, A. Wakamiya, S. Yamaguchi, K. S. Kim, Z. S. Yoon, D. Kim, A. Osuka, *J. Am. Chem. Soc.* **2006**, *128*, 7670 – 7678; c) M. Kitamura, M. Yamakawa, H. Oka, S. Suga, R. Noyori, *Chem. Eur. J.* **1996**, *2*, 1173 – 1181; d) P. L. Arnold, J.-C. Buffet, R. Blaudeck, S. Sujecki, C. Wilson, *Chem. Eur. J.* **2009**, *15*, 8241 – 8250.

[9] a) Y. Jin, C. Yu, R. J. Denman, W. Zhang, *Chem. Soc. Rev.* **2013**, *42*, 6634 – 6654; b) J.-M. Lehn, *Chem. Eur. J.* **1999**, *5*, 2455 – 2463.

[10] L. L. Schafer, T. D. Tilley, *J. Am. Chem. Soc.* **2001**, *123*, 2683 – 2684.

[11] S. W. Sisco, J. S. Moore, *Chem. Sci.* **2014**, *5*, 81 – 85.

[12] a) C. Tsiamantas, X. de Hatten, C. Douat, B. Kauffmann, V. Maurizot, H. Ihara, M. Takafuji, N. Metzler-Nolte, I. Huc, *Angew. Chem. Int. Ed.* **2016**, *55*, 6848 – 6852; *Angew. Chem.* **2016**, *128*, 6962 – 6966; b) P. T. Corbett, J. K. M. Sanders, S. Otto, *Chem. Eur. J.* **2008**, *14*, 2153 – 2166; c) P. T. Corbett, J. K. M. Sanders, S. Otto, *J. Am. Chem. Soc.* **2005**, *127*, 9390 – 9392.

[13] a) H. Qu, Y. Wang, Z. Li, X. Wang, H. Fang, Z. Tian, X. Cao, *J. Am. Chem. Soc.* **2017**, *139*, 18142 – 18145; b) Y. Wang, H. Fang, I. Tranca, H. Qu, X. Wang, A. J. Markvoort, Z. Tian, X. Cao, *Nat. Commun.* **2018**, *9*, 488; c) Y. Wang, H. Fang, W. Zhang, Y. Zhuang, Z. Tian, X. Cao, *Chem. Commun.* **2017**, *53*, 8956 – 8959; d) P. Zhang, X. Wang, W. Xuan, P. Peng, Z. Li, R. Lu, S. Wu, Z. Tian, X. Cao, *Chem. Commun.* **2018**, *54*, 4685 – 4688; e) X. Wang, Y. Wang, H. Yang, H. Fang, R. Chen, Y. Sun, N. Zheng, K. Tan, X. Lu, Z. Tian, X. Cao, *Nat. Commun.* **2016**, *7*, 12469; f) H. Qu, X. Tang, X. Wang, Z. Li, Z. Huang, H. Zhang, Z. Tian, X. Cao, *Chem. Sci.* **2018**, *9*, 8814 – 8818; g) X. Wang, P. Peng, W. Xuan, Y. Wang, Y. Zhuang, Z. Tian, X. Cao, *Org. Biol. Chem.* **2018**, *16*, 34 – 37; h) T. Wang, Y.-F. Zhang, Q.-Q. Hou, W.-R. Xu, X.-P. Cao, H.-F. Chow, D. Kuck, *J. Org. Chem.* **2013**, *78*, 1062 – 1069; i) D. Beaudoin, F. Rominger, M. Mastalerz, *Angew. Chem. Int. Ed.* **2017**, *56*, 1244 – 1248; *Angew. Chem.* **2017**, *129*, 1264 – 1268; j) M. Petryk, K. Biniek, A. Janiak, M. Kwit, *CrystEngComm* **2016**, *18*, 4996 – 5003; k) A. G. Slater, M. A. Little, M. E. Briggs, K. E. Jelfs, A. I. Cooper, *Mol. Syst. Des. Eng.* **2018**, *3*, 223 – 227.

[14] H. Takahagi, S. Fujibe, N. Iwasawa, *Chem. Eur. J.* **2009**, *15*, 13327 – 13330.

[15] W. Wang, A. D. Shaller, A. D. Q. Li, *J. Am. Chem. Soc.* **2008**, *130*, 8271 – 8279.

[16] N. Ponnuswamy, F. B. L. Cougnon, G. D. Pantoş, J. K. M. Sanders, *J. Am. Chem. Soc.* **2014**, *136*, 8243 – 8251.

[17] H. Jędrzejewska, M. Wierzbicki, P. Cmoch, K. Rissanen, A. Szumna, *Angew. Chem. Int. Ed.* **2014**, *53*, 13760 – 13764; *Angew. Chem.* **2014**, *126*, 13980 – 13984.

[18] a) M. Mastalerz, *Acc. Chem. Res.* **2018**, *51*, 2411 – 2422; b) V. Santolini, M. Miklitz, E. Berardo, K. E. Jelfs, *Nanoscale* **2017**, *9*, 5280 – 5298; c) N. M. Rue, J. Sun, R. Warmuth, *Isr. J. Chem.* **2011**, *51*, 743 – 768; d) G. Zhang, M. Mastalerz, *Chem. Soc. Rev.* **2014**, *43*, 1934 – 1947; e) M. Mastalerz, *Synlett* **2013**, *24*, 781 – 786; f) R. D. Mukhopadhyay, Y. Kim, J. Koo, K. Kim, *Acc. Chem. Res.* **2018**, *51*, 2730 – 2738; g) F. Beuerle, B. Gole, *Angew. Chem. Int. Ed.* **2018**, *57*, 4850 – 4878; *Angew. Chem.* **2018**, *130*, 4942 – 4972.

[19] a) S. Klotzbach, F. Beuerle, *Angew. Chem. Int. Ed.* **2015**, *54*, 10356 – 10360; *Angew. Chem.* **2015**, *127*, 10497 – 10502; b) F. Beuerle, S. Klotzbach, A. Dhara, *Synlett* **2016**, *27*, 1133 – 1138; c) T. H. G. Schick, F. Rominger, M. Mastalerz, *J. Org. Chem.* **2020**, *85*, 13757 – 13771; d) K. Acharyya, S. Mukherjee, P. S. Mukherjee, *J. Am. Chem. Soc.* **2013**, *135*, 554 – 557; e) K. Acharyya, P. S. Mukherjee, *Chem. Eur. J.* **2014**, *20*, 1646 – 1657; f) K. Acharyya, P. S. Mukherjee, *Chem. Commun.* **2015**, *51*, 4241 – 4244; g) T. Jiao, G. Wu, L. Chen, C.-Y. Wang, H. Li, *J. Org. Chem.* **2018**, *83*, 12404 – 12410; h) M. Kołodziejski, A. R. Stefankiewicz, J.-M. Lehn, *Chem. Sci.* **2019**, *10*, 1836 – 1843; i) R. L. Greenaway, V. Santolini, A. Pulido, M. A. Little, B. M. Alston, M. E. Briggs, G. M. Day, A. I. Cooper, K. E. Jelfs, *Angew. Chem. Int. Ed.* **2019**, *58*, 16275 – 16281; *Angew. Chem.* **2019**, *131*, 16421 – 16427; j) Z. Yang, J.-M. Lehn, *J. Am. Chem. Soc.* **2020**, *142*, 15137 – 15145; k) V. Abet, F. T. Szczypiński, M. A. Little, V. Santolini, C. D. Jones, R. Evans, C. Wilson, X. Wu, M. F. Thorne, M. J. Bennison, P. Cui, A. I. Cooper, K. E. Jelfs, A. G. Slater, *Angew. Chem. Int. Ed.* **2020**, *59*, 16755 – 16763; *Angew. Chem.* **2020**, *132*, 16898 – 16906; l) V. Abet, F. T. Szczypiński, M. A. Little, V. Santolini, C. D. Jones, R. Evans, C. Wilson, X. Wu, M. F. Thorne, M. J. Bennison, P. Cui, A. I. Cooper, K. E. Jelfs, A. G. Slater, *Angew. Chem. Int. Ed.* **2020**, *59*, 20272 – 20272; *Angew. Chem.* **2020**, *132*, 20447 – 20447; m) K. Acharyya, P. S. Mukherjee, *Angew. Chem. Int. Ed.* **2019**, *58*, 8640 – 8653; *Angew. Chem.* **2019**, *131*, 8732 – 8745.

[20] a) F. J. Rizzuto, J. R. Nitschke, *J. Am. Chem. Soc.* **2020**, *142*, 7749 – 7753; b) A. Kumar, P. S. Mukherjee, *Chem. Eur. J.* **2020**, *26*, 4842 – 4849.

[21] D. Xu, R. Warmuth, *J. Am. Chem. Soc.* **2008**, *130*, 7520 – 7521.

[22] J. C. Duff, E. J. Bills, *J. Chem. Soc. (Resumed)* **1934**, 1305 – 1308.

[23] a) P. Wagner, F. Rominger, M. Mastalerz, *Angew. Chem. Int. Ed.* **2018**, *57*, 11321 – 11324; *Angew. Chem.* **2018**, *130*, 11491 – 11494; b) P. Wagner, F. Rominger, T. Oeser, M. Mastalerz, *J. Org. Chem.* **2020**, *85*, 3981 – 3989.

[24] E. L. Eliel, S. H. Wilen, *Stereochemistry of Organic Compounds*, Wiley, New York, **1994**.

[25] a) F. Furche, R. Ahlrichs, C. Wachsmann, E. Weber, A. Sobanski, F. Vögtle, S. Grimme, *J. Am. Chem. Soc.* **2000**, *122*, 1717 – 1724; b) H. Tanaka, M. Ikenosako, Y. Kato, M. Fujiki, Y. Inoue, T. Mori, *Commun. Chem.* **2018**, *1*, 38.

[26] P. M. Neumann, *The Mathematical Scientist* **1979**, *4*, 133 – 141.

[27] Unfortunately, for the here described system, we were unable to obtain experimental thermodynamic data since the characteristic signals for the enantiopure and *meso* cages were too broad to precisely determine their respective ratios by integration of ^{1}H NMR spectra recorded at variable temperatures to apply a van't Hoff plot (see Reference [13i]).

[28] Calculated using $K_{eq}=e^{\frac{-\Delta H_R}{RT}}$ with $T=333.15$ K (60 °C).

[29] a) V. Santolini, G. A. Tribello, K. E. Jelfs, *Chem. Commun.* **2015**, *51*, 15542 – 15545; b) K. E. Jelfs, X. Wu, M. Schmidtmann, J. T. A. Jones, J. E. Warren, D. J. Adams, A. I. Cooper, *Angew. Chem. Int. Ed.* **2011**, *50*, 10653 – 10656; *Angew. Chem.* **2011**, *123*, 10841 – 10844.

[30] a) A. Ben-Naim, *J. Chem. Educ.* **2011**, *88*, 594 – 596; b) S.-K. Lin, *J. Chem. Inf. Comput. Sci.* **1996**, *36*, 367 – 376.

[31] P. Skowronek, B. Warżajtis, U. Rychlewska, J. Gawroński, *Chem. Commun.* **2013**, *49*, 2524 – 2526.

[32] a) A. Spek, *Acta Crystallogr. Sect. D* **2009**, *65*, 148 – 155; b) P. van der Sluis, A. L. Spek, *Acta Crystallogr. Sect. A* **1990**, *46*, 194 – 201.

[33] G. Zhang, O. Presly, F. White, I. M. Oppel, M. Mastalerz, *Angew. Chem. Int. Ed.* **2014**, *53*, 1516 – 1520; *Angew. Chem.* **2014**, *126*, 1542 – 1546.

[34] K. Su, W. Wang, S. Du, C. Ji, M. Zhou, D. Yuan, *J. Am. Chem. Soc.* **2020**, *142*, 18060 – 18072.

[35] J. Koo, I. Kim, Y. Kim, D. Cho, I.-C. Hwang, R. D. Mukhopadhyay, H. Song, Y. H. Ko, A. Dhamija, H. Lee, W. Hwang, S. Kim, M.-H. Baik, K. Kim, *Chem* **2020**, *6*, 3374 – 3384.

[36] a) T. Hasell, S. Y. Chong, K. E. Jelfs, D. J. Adams, A. I. Cooper, *J. Am. Chem. Soc.* **2012**, *134*, 588 – 598; b) T. Hasell, S. Y. Chong, M. Schmidtmann, D. J. Adams, A. I. Cooper, *Angew. Chem. Int. Ed.* **2012**, *51*, 7154 – 7157; *Angew. Chem.* **2012**, *124*, 7266 – 7269; c) T. Hasell, M. A. Little, S. Y. Chong, M. Schmidtmann, M. E. Briggs, V. Santolini, K. E. Jelfs, A. I. Cooper, *Nanoscale* **2017**, *9*, 6783 – 6790; d) J. T. A. Jones, T. Hasell, X. Wu, J. Bacsa, K. E. Jelfs, M. Schmidtmann, S. Y. Chong, D. J. Adams, A. Trewin, F. Schiffman, F. Cora, B. Slater, A. Steiner, G. M. Day, A. I. Cooper, *Nature* **2011**, *474*, 367 – 371.

[37] C. J. Pugh, V. Santolini, R. L. Greenaway, M. A. Little, M. E. Briggs, K. E. Jelfs, A. I. Cooper, *Cryst. Growth Des.* **2018**, *18*, 2759 – 2764.

[38] a) L. J. Barbour, *Chem. Commun.* **2006**, 1163 – 1168; b) M. J. Turner, J. J. McKinnon, D. Jayatilaka, M. A. Spackman, *CrystEngComm* **2011**, *13*, 1804 – 1813; c) *CrystalExplorer* (Version 17.5), S. K. Wolff, D. J. Grimwood, J. J. McKinnon, M. J. Turner, D. Jayatilaka, M. A. Spackman, University of Western Australia, **2017**.

[39] a) M. Mastalerz, I. M. Oppel, *Angew. Chem. Int. Ed.* **2012**, *51*, 5252 – 5255; *Angew. Chem.* **2012**, *124*, 5345 – 5348; b) J. C. Lauer, W.-S. Zhang, F. Rominger, R. R. Schröder, M. Mastalerz, *Chem. Eur. J.* **2018**, *24*, 1816 – 1820.

[40] a) S. Jiang, K. E. Jelfs, D. Holden, T. Hasell, S. Y. Chong, M. Haranczyk, A. Trewin, A. I. Cooper, *J. Am. Chem. Soc.* **2013**, *135*, 17818 – 17830; b) S. M. Elbert, F. Rominger, M. Mastalerz, *Chem. Eur. J.* **2014**, *20*, 16707 – 16720.

[41] a) M. W. Schneider, I. M. Oppel, H. Ott, L. G. Lechner, H.-J. S. Hauswald, R. Stoll, M. Mastalerz, *Chem. Eur. J.* **2012**, *18*, 836 – 847; b) A. G. Slater, M. A. Little, A. Pulido, S. Y. Chong, D. Holden, L. Chen, C. Morgan, X. Wu, G. Cheng, R. Clowes, M. E. Briggs, T. Hasell, K. E. Jelfs, G. M. Day, A. I. Cooper, *Nat. Chem.* **2017**, *9*, 17 – 25; c) G. Zhang, O. Presly, F. White, I. M. Oppel, M. Mastalerz, *Angew. Chem. Int. Ed.* **2014**, *53*, 5126 – 5130; *Angew. Chem.* **2014**, *126*, 5226 – 5230; d) M. W. Schneider, I. M. Oppel, A. Griffin, M. Mastalerz, *Angew. Chem. Int. Ed.* **2013**, *52*, 3611 – 3615; *Angew. Chem.* **2013**, *125*, 3699 – 3703.

[42] A. Avellaneda, P. Valente, A. Burgun, J. D. Evans, A. W. Markwell-Heys, D. Rankine, D. J. Nielsen, M. R. Hill, C. J. Sumby, C. J. Doonan, *Angew. Chem. Int. Ed.* **2013**, *52*, 3746 – 3749; *Angew. Chem.* **2013**, *125*, 3834 – 3837.

[43] Deposition Number(s) 2022632, 2022635, 2022636, 2022633, 2022634 and 2022637 (for (−)-(*P*)-**2**, (+)-(*M*)-**2**, (±)-(*P,M*)-**4** (crystals from $CDCl_3$), (±)-(*P,M*)-**4** (crystals from DCM) and (+)-(*P*)-**4**, respectively) contain(s) the supplementary crystallographic data for this paper. These data are provided free of charge by the joint Cambridge Crystallographic Data Centre and Fachinformationszentrum Karlsruhe Access Structures service www.ccdc.cam.ac.uk/structures.

Manuscript received: December 14, 2020
Revised manuscript received: January 21, 2021
Accepted manuscript online: January 21, 2021
Version of record online: March 8, 2021

